Acta Polytechnica **63**(6):419–429, 2023
https://doi.org/10.14311/AP.2023.63.0419

Published by the Czech Technical University in Prague

ENHANCEMENT OF POWER TRANSFER CAPACITY OF TRANSMISSION NETWORK USING MULTILEVEL MULTIFUNCTION INVERTER

Kiran Nathgosavi*, Prasad Joshi

Shivaji University, Rajarambapu Institute of Technology, Department of Electrical Engineering, Sakharale, 415414 Maharashtra, India

* corresponding author: kiran.nathgosavi@ritindia.edu

Abstract. This article presents a multilevel multifunction inverter (MLMFI) with a novel controller for the grid-connection of a solar array. The aim of this work is to improve the technology of the power transfer capacity of existing transmission lines in order to alleviate the current energy crisis. An effective mathematical modelling of an MLMFI configuration having two series-connected H-bridges per phase with isolated solar arrays is presented. A novel closed-loop controller is proposed for reference signal generation using the PWM technique. With the proposed controller, the power flow in a transmission line is analysed for daytime and nighttime conditions. The proposed controller performance was tested on a realistic single-machine infinite-bus power system with midpoint MLMFI using MATLAB simulation software. The proposed MLMFI-based solar array enhanced the stable power transfer limit of a transmission line. A comparative analysis between conventional and proposed controllers for power flow and transient stability studies was also presented. The proposed MLMFI results were validated by developing an experimental model.

Keywords: Damping controller, multilevel inverter, grid connected photovoltaic solar systems, transient stability, transmission capacity.

1. Introduction

Electricity demand in the power system in India is increasing due to the rapid development of industry, households, and other sectors. Thus, there is a need to generate more power and transmit it to the customers to fulfil their demand. Because of development and promotion from the government in the form of subsidies, solar system utilisation increased with respect to other renewable sources [1, 2]. However, the irregular distribution of solar energy due to geographical conditions causes the installation of large scale photovoltaic (PV) systems in remote or desert areas where the sun's radiation is available in sufficient amounts [3]. It results in a high grid impedance because of the long-distance transmission network. This results in weak points in the connection of renewable energy in the system [4, 5]. The effect of high impedance can be eliminated and the power transfer capacity of transmission networks can be improved by using power electronics-based transmission systems, such as High Voltage Direct Current (HVDC) networks [6] and Flexible Alternative Current Transmission System (FACTS) devices [7]. Transmission line efficiency and power transfer capacity enhancement are presented in [8] by using a Synchronous Series Compensator (SSSC) with a comparative analysis between compensated and uncompensated transmission lines. The power transfer ability that gets enhanced in a transmission and distribution network using Thyristor Controlled Series Capacitors (TCSC) is presented in [9]. The series FACTS controller directly controls the active power flow by controlling the line reactance. The shunt FACTS devices control it indirectly by controlling the PCC voltage and phase angle. There are system stability and power quality issues arising from the interactions between the HVDC systems, FACTS devices, and grid-connected renewable sources [10–13]. This results in oscillations in the system and makes it instable. Therefore, to improve the power transfer capability of the transmission grid, the controllability of PV inverters needs to be improved so that they can perform multiple operations, such as reactive power control, voltage control, and power factor correction. This results in reducing the cost of upgrading the transmission grid.

PV plants and FACTS devices have a common element, the inverter; therefore, PV plants can be operated as FACTS devices [14], which can be useful for both real power generation and reactive power compensation [15]. The PV inverter is used as a STATCOM, which is also called a PV-STATCOM. In addition to that, the transient stability of the system is also increased by implementing a PV plant as a FACTS device [16], as there is greater power transfer in stable operating conditions. There are different types of inverters. The conventional two-level inverter develops a square wave voltage as an output with a high switching frequency. This output has a high harmonic content, so it requires large dimensional filters [17]. However, the power loss and extra costs required for carrying the total harmonic distortion

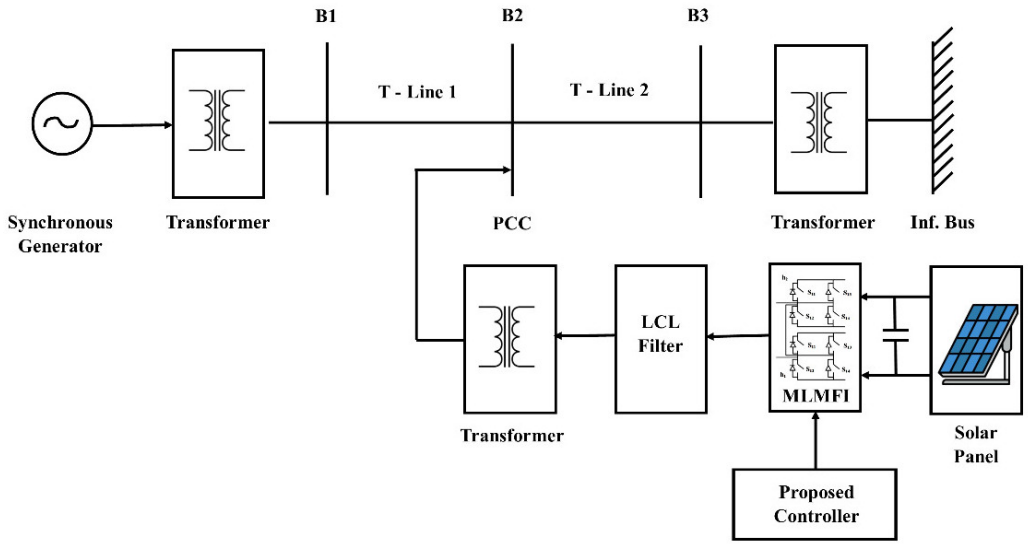

Figure 1. Block diagram of the proposed system.

(THD) to the permitted limit [18] are considerably high. Therefore, multilevel inverters (MLIs) are dominant in this field due to the improved output power quality and efficiency [19, 20]. MLI generates a staircase output waveform, which is nearly sinusoidal and has a lesser amount of THD. There are various popular MLI topologies described with enhancements in the conventional H-bridge structure, such as HERIC, H-6, and H-5 [21, 22]. These MLIs require supplementary filter inductors. Hence, they are larger and less suited for grid-connected applications. In addition, the quantity of active switches in series with the load during the procedure increases the conduction loss. A five-level H-bridge MLI is reported in [22]. This topology has utilised the bidirectional power flow by using a bidirectional switch in the essential terminal. This makes the configuration well suited for reactive power control and grid-connected applications.

Flexible power control techniques for PV plants are split into two groups: centralised control [23–25] and decentralised control [26, 27]. In addition, various PWM techniques and PI controller implementation with signal processing and modulation index were presented in [28–31], The centralised control required an additional communication network, which increased the cost and complexity of the system. The PV inverter is used to regulate reactive power based on remote voltage and active power to mitigate the voltage variation produced by the injected power [32–35].

Despite the variety of power controls that have been extensively studied, it has been found that the reactive power controller of a normal two-level inverter has a limit on the utilisation of the solar array during the night. Hence, there is a research scope mainly focused on effective control techniques to enhance the power transfer capability of the transmission network during the day and at night. This paper proposes a novel multilevel multifunction inverter (MLMFI) controller to enhance the power transfer capability of transmission grid. The proposed controller for MLMFI uses the PV system both during the day and at night. The main contributions of this paper can be summarised as follows: 1) Modelling of the MLMFI for PV systems; 2) a novel controller to enhance power transfer capacity; and 3) a comparative analysis of power transfer capacity.

The paper is structured as follows: Section 2 describes the modelling of the MLMFI and its controller. Section 3 presents the simulation and its results. Experimental validation is given in Section 4, and Section 5 contains a conclusion.

2. Materials and methods

2.1. Proposed system configuration

The block diagram of the proposed system is shown in Figure 1 which consists of a large synchronous generator (1110 MVA) having a DC1A-type excitation system. The transmission lines T-line 1 and T-line 2 are of the lumped pi circuit type. The PV solar system (100 MW) is considered an equivalent multilevel voltage source inverter. It has a controlled DC source which obeys the I-V characteristics of the PV system. An incremental conductance maximum power point tracking algorithm is integrated with the main inverter controller. This MPPT algorithm is used to extract the maximum power from the solar system at any time. The extracted power is stored in the DC capacitor (200 F) at the input side of the inverter.

This large DC capacitor also performs a function to reduce DC-side ripples. During night time, the solar panels get disconnected and the DC capacitors get charged by taking a small amount of real power from the grid. The multilevel inverter is five-level cascaded H-bridge type. It has two series of connected

Component	Rating
Synchronous Generator	1110 MVA with DC1A - exciter
T-Line 1 & 2	100 km, 400 kV
Transformer 1 & 3	1110 MVA, 22/400 kV, Star-Star
Transformer 2	100 MVA, 0.208/400 kV, Delta-Star
LCL filter	$L_i = 500$ mH, $C_f = 100$ µF, $L_g = 500$ mH
MLMFI Inverter	100 MVA, 220 V
Solar Array	100 MVA

TABLE 1. Proposed system parameters

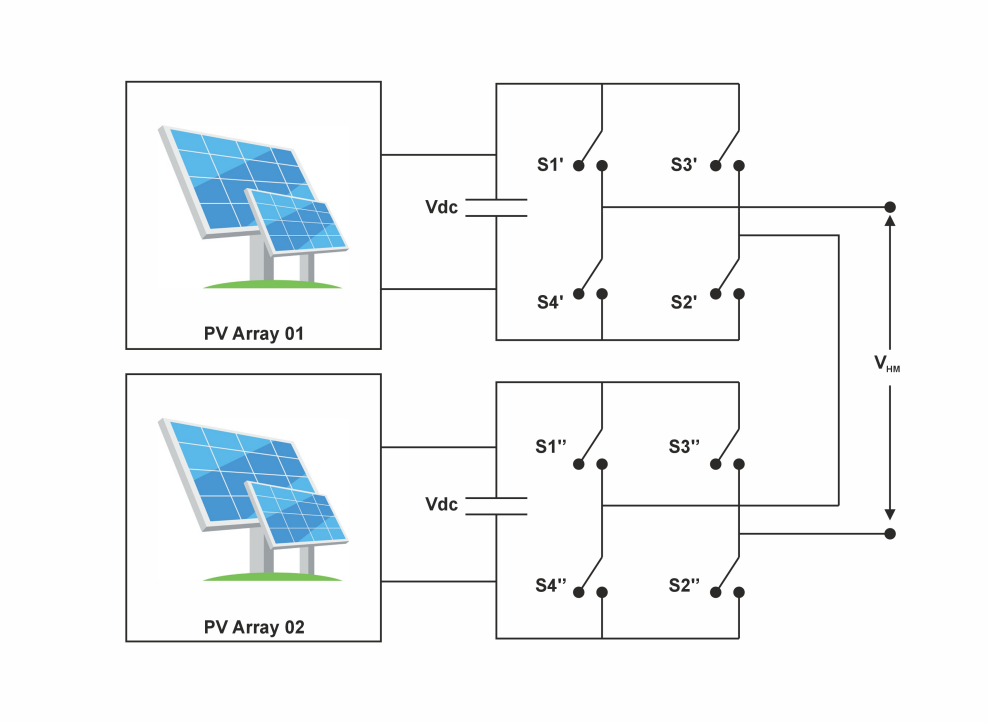

FIGURE 2. BFive-level cascaded H-bridge inverter.

H-bridges per phase with isolated PV panels. The multilevel inverter converts DC voltage into a staircase variable-width pulsating voltage which gets filtered by an L-C-L filter. The parameters of the proposed system are listed in Table 1.

2.2. MODELLING OF MLMFI AND ITS CONTROLLER

The multilevel inverter offers various benefits over a two-level inverter. MLI improves power quality and efficiency, reduces electromagnetic interference, harmonics, and voltage stress on power switches. Currently, multilevel inverters are used in various applications, such as flexible AC transmission system devices, energy storage systems, electric vehicle drives, and renewable energy integrations. The multilevel inverter has three distinctive topologies: diode clamped, flying capacitor, and cascaded H-bridge. There are various advantages of the cascaded H-bridge multilevel inverter over other topologies. It consists of a series of H-bridges with separate DC sources. Hence the cascaded H-bridge inverter becomes a more prominent topology for interfacing distributed generators or renewable energy sources to the grid. Currently, it is expected that the grid-connected inverter will perform various tasks, such as active power transfer, harmonic mitigation, and reactive power compensation, hence the term multifunction inverter. These multiple functions can be performed by a properly designed controller.

2.2.1. MATHEMATICAL MODELING OF MLMFI:

It is considered that the cascaded H-bridge multilevel inverter consists of H-bridges connected in series having a separate string of PV panels as shown in Figure 2. This is a single-stage grid-connected PV system. Here, it is considered that both the PV strings provide the same voltage to the DC link capacitor of the H-bridge.

The minimum amplitude of the DC bus capacitance with time constant is given by Equations (1) and (2). Where two 100 F capacitors are connected in series to meet the value of the DC bus. The total capacity of the PV array is 100 MW. Therefore, the multilevel converter produces an output voltage with m levels.

S1'	S4'	S3'	S2'	S1"	S4"	S3"	S2"	V_{HM}
1	0	0	1	1	0	0	1	$+2V_H$
1	0	0	1	0	1	0	1	$+V_H$
0	1	0	1	0	1	0	1	0
0	1	1	0	0	1	0	1	$-V_H$
0	1	1	0	1	1	1	0	$-2V_H$

TABLE 2. Switching pattern of five-level MLMFI.

$$C_{bus} = \frac{4\,P}{V_{DC\_min}^2}\,t_1, \tag{1}$$

$$t_1 = \frac{1}{4\,f_g}. \tag{2}$$

The output waveform of the proposed cascaded H-bridge inverter is having low harmonic content, reducing the need for filtering. Here, V_{HM} is the output voltage and I_{HM} is the output current of m level inverter, which is stated in Equations (3) and (4). This means that the output is having five values $(+2V_H, +V_H, 0, -V_H, -2V_H)$ depending on the switching pattern, which is shown in Table 2. Where 1 represents ON and 0 represents OFF. It means that the output AC voltage waveform has $2m + 1$ levels.

Dynamic performance of the PV array is described by considering a nonlinear voltage-current relation. Let us consider that the V_{cm} is the voltage across the m^{th} H-bridge DC link capacitor and I_L is the current generated by the m^{th} H-bridge.

$$V_{hm} = u_m V_{\mathrm{cm}}, \tag{3}$$

$$i_{hm} = u_m i_L, \tag{4}$$

where, u_m is the control signal for all H-bridges operated under the five-level modulation so that the control signal is limited to the values (−2, −1, 0, 1, 2).

Equation (5) represents the power capacity of the inverter when it is considered to be a lossless inverter

$$V_{cm} i_{hm} = V_{hm} i_L. \tag{5}$$

The output voltage of cascaded H-bridge inverter V_H is given by Equation (6), which clearly shows that the output is dependent on the output levels.

$$V_H = \sum_{m=1}^{n} V_{HM} = \sum_{m=1}^{n} u_m v_{\mathrm{cm}}. \tag{6}$$

The system dynamics are given by differential Equations (7), (8), and (9).

$$C_m \frac{dv_{cm}}{dt} = i_{pVm} - u_m i_L, \tag{7}$$

$$L\frac{di_L}{dt} = \sum_{m=1}^{n} u_m v_{cm} - v_s(t), \tag{8}$$

where v_s is the grid voltage which can be expressed as

$$v_s = v\sin(wt), \tag{9}$$

where w is the angular frequency of the grid.

AC output current dynamic performance of the MLMFI is expressed by the differential equation

$$L\frac{di_a}{dt} + Ri_a = v_{0a}(t) - v_{pcca}(t), \tag{10}$$

where v_{0a} are control signals and v_{pcca} are the PCC disturbance inputs.

The output LCL filter transfer function of a multilevel multifunction inverter is expressed by Equation (11)

$$G_i(s) = \frac{i_{a(S)}}{v_{a(S)}} = \frac{1}{L_S + R}. \tag{11}$$

The controller of the cascaded multilevel inverter has two main outcomes:

1. PV array should be used as to extract the maximum power regardless of environmental conditions.
2. Feed all generated power into the grid with minimum harmonics and unity power factor.

The first outcome is achieved through a voltage control loop by regulating the respective capacitor voltage v_{cm} to reference the voltage value provided by the MPPT algorithm. The second outcome is achieved by injecting the output current i_L to follow the current reference i_L^* expressed by Equation (12) with fast transient response and zero steady-state error.

$$i_L^* = k(t)v_s(t) = K(t)V\sin(wt). \tag{12}$$

The current amplitude varies with time so that the power calculation is only possible when the inverter output current is at the reference value. The average and instantaneous power are expressed by Equations (12) and (13).

$$P_{avg} = \frac{1}{T_s}\int_{k-1T_S}^{kT}\sum_{m=1}^{n} i_{pVm}(t)v_{Cm}(t)dt, \tag{13}$$

where k is the time instant.

As the input DC power and environmental conditions depend on the solar array, the instantaneous DC power is

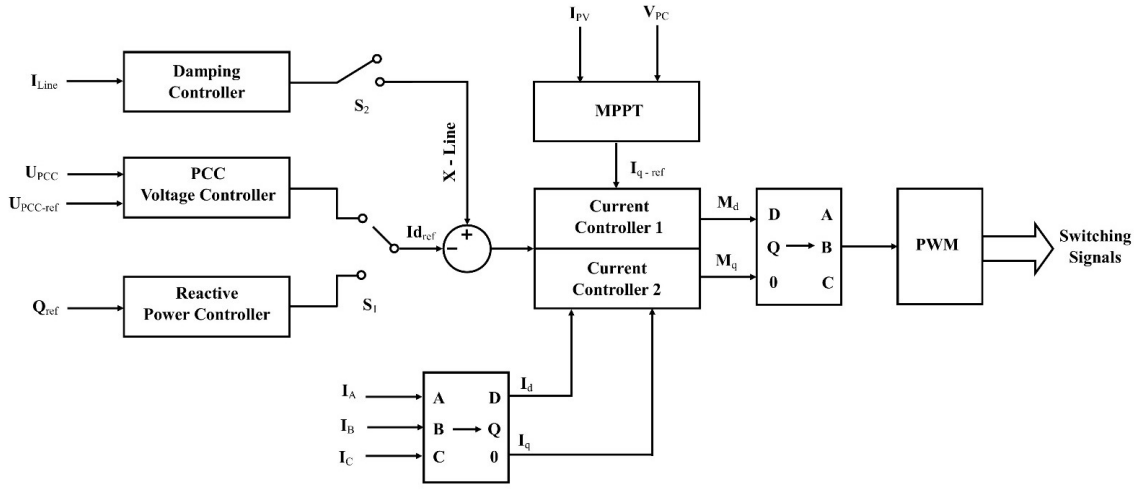

FIGURE 3. Proposed control system for MLMFI.

$$P = \sum_{m=1}^{n} i_{PVm(k-1)}\, v_{cm(k-1)}, \tag{14}$$

where m is the integer representing the number of H-bridges.

From the above assumptions, the current reference is given by Equation (15).

$$i_L^* = K(k-1)V\sin(wt). \tag{15}$$

Therefore, the output current of the current controller should follow the current reference given by Equation (15) in order to transfer all the generated DC power to the grid through the MLMFI. In addition, the maximum power transfer is possible only if the voltage controller is set to its maximum value.

2.2.2. MODELLING OF PROPOSED CONTROLLER

The main objective of the proposed controller is to produce a reference signal. The controller has two current control loops in the d-q-0 system. These current control loops have the grid voltage and load current as input signals. By using Clark's transformation, these three-phase instantaneous quantities get converted into two phase quantities as shown in Figure 3. Three phase instantaneous load current is expressed by the Equations (16), 17), and 18).

$$i_{La} = \sum I_{La}\sin(wt - \phi_a), \tag{16}$$

$$i_{Lb} = \sum I_{Lb}\sin\left\{\left(wt - \frac{2\pi}{3}\right) - \phi_b\right\}, \tag{17}$$

$$i_{Lc} = \sum I_{Lc}\sin\left\{\left(wt + \frac{2\pi}{3}\right) - \phi_c\right\}. \tag{18}$$

Now, these three-phase current instantaneous values get converted into stationary reference frame values using Clarks transformation expressed in Equation (19).

$$\begin{bmatrix} i_d \\ i_q \\ 0 \end{bmatrix} = \frac{2}{3}\begin{bmatrix} 1 & -0.5 & -0.5 \\ 0 & 1.22 & -1.22 \\ 0.5 & 0.5 & 0.5 \end{bmatrix}\begin{bmatrix} i_{La} \\ i_{Lb} \\ i_{Lc} \end{bmatrix}. \tag{19}$$

It is considered that the voltage vector control is in-phase with the quadrature axis. Therefore, the Q_{ref} is proportional to i_d only to set i_{dref} for the current control loop 1 and send it to PI-1 as shown in Figure 3. The DC link voltage is controlled by using quadrature axis component i_q using the current controller loop 2 and sending it to PI-2. The MPPT get integrated with PI-3 to the current controller loop-2 to deliver the available real power to grid. Switching pulses are generated with the help of level sift PWM technique having 5-kHz carrier signal. The reference sinusoidal modulating signals shown in Figure 3 are converted from d-q modulating components of m_d and m_q as given in Equation (20).

$$\begin{bmatrix} i_a^* \\ i_b^* \\ i_c^* \end{bmatrix} = \begin{bmatrix} 1 & 0 & 1 \\ -0.5 & 1.22 & 1 \\ -0.5 & -1.22 & 1 \end{bmatrix}\begin{bmatrix} m_d \\ m_q \\ 0 \end{bmatrix}. \tag{20}$$

There is an effective way to set Q_{ref} by incorporating a PCC voltage controller to enhance the power transfer capacity of a system. To achieve a better reactive power exchange between the PV system and the grid, Id_{ref} is determined by comparing the measured voltage (V_{pcc}) with preset reference voltage (V_{pcc_ref}).

The error is then passed through the PI-4 regulator instead of the reactive power Q Channel control. The rest of the controller remains the same. Because of this modification, current control loop 1 regulates the PCC voltage, and current control loop 2 maintains the DC link voltage constant as well as the actual power transfer to the grid. The set point PCC voltage defines the amount of reactive power exchange between the PV system and the grid.

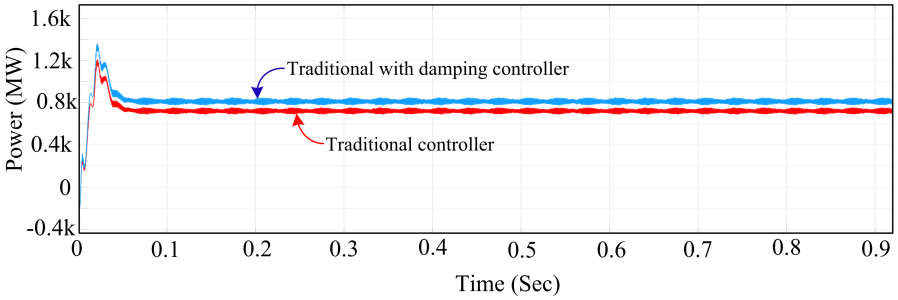

Figure 4. Power transfer capacity of system during the day.

Condition		Gen. bus power [MWAr]	Inf. bus power [MW]	PCC parameters Psolar [MW]	Qsolar [MWAr]	Vpcc [pu]
Daytime	Reactive power controller only	730 851	−725 −839	19 19	−0.50 −0.06	1.010 1.000
	Reactive power with damping controller	719 861	−786 −917	91 91	−0.20 −0.20	1.008 0.994
Nighttime	Reactive power controller only	731	−708	0	0.00	1.010
	Reactive power with damping controller	850	−819	0	−0.20	1.000

Table 3. Power and voltage for reactive power controller and damping controller.

In addition, the proposed controller, as shown in Figure 3, is designed to dampen the rotor oscillations of the synchronous generator so as to improve the transient stability of the system. This can be achieved by considering the line current magnitude as a control signal and adding its output to Id_{ref}. The dynamic behaviour of this is expressed by a transfer function in Equation (21).

$$G(s) = K\left(\frac{sT_w}{1+sT_w}\right)\left(\frac{1+sT_1}{1+sT_2}\right), \qquad (21)$$

where, K is the gain, T_w is the washout time constant that is to be selected in order to allow oscillations, and T_1 and T_2 are time constants to obtain a fast settling time. The controller parameters, set by trial and error, are given in Table 4. The proposed controller is designed by considering a base generator operating power, which is also considered a transient stability limit when the solar system is disconnected.

Parameter	Value
PI-1	$K_p = 1, T_i = 0.0015$
PI-2	$K_p = 1, T_i = 0.1$
PI-3	$K_p = 2, T_i = 0.2$
PI-4	$K_p = 10, T_i = 0.0015$
Damping controller	$T_w = 0.1, K = 1.0,$ $T_1 = 1, T_2 = 0.37$

Table 4. Proposed controller parameters.

3. Simulation and Results

The Simulation of the proposed system is carried out in MATLAB simulation software. Through a transient stability study of the LLL-G fault, it is calculated that at 5 % damping ratio, the rotor will have 0.95 Hz oscillations. From the simulation results, it can be seen that the PCC voltage is limited within 1.1 p.u. and a settling time of 10 s is required for oscillations. The transient stability study is important to find the maximum stable power generation unit of a distribution generator (DG). The proposed system is to be analysed in two different cases based on reference reactive power (Q_{ref}). Case-I: Q_{ref} is determined from voltage vector control, and Case-II: Q_{ref} is determined from PCC voltage.

3.1. Case-I

At night, the solar system becomes inactive. In that condition, the generator output is 731 MW, which is to be considered here as a base value for the system analysis. The stable power transfer is shown in Table 3, where the negative sign represents power drown and the positive sign represents power delivered in both real and reactive power.

If the reactive power controller is used along with the damping controller at night, then the full rating of the solar inverter is used for reactive power control, and rotor mode oscillations get effectively damped out. Figure 4 shows the power transfer capacity of

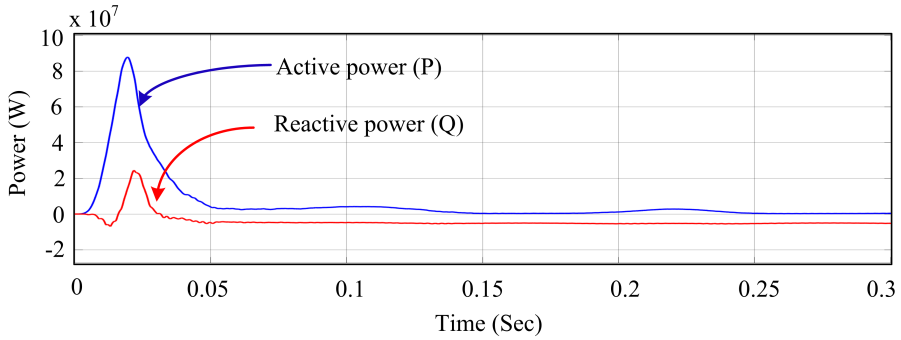

FIGURE 5. Capacitor charging power during night.

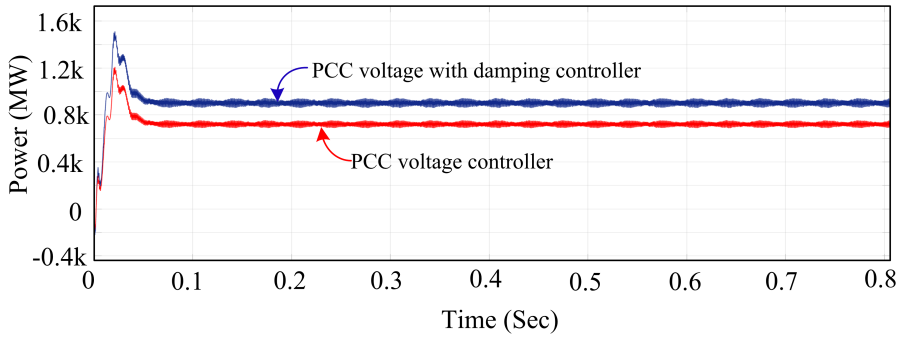

FIGURE 6. Power transfer capacity of system during the day.

the system with and without the proposed controller. In this condition, a very small amount of power flows from the grid to the solar system, as shown in Table 3. Negative sign is used to indicate the use of power.

This purpose of this power flow is to charge the DC-link capacitor and maintain its voltage constant so that the PV system acts as a FACTS device with a damping controller. At night, the reference DC-link voltage is set based on the MPP during the day. The performance of the solar system, taking into account the energy exchange, is shown in Figure 5.

During the day, the reactive power controller does not have much effect on improving the power transfer capacity, but if the reactive power controller is considered with a damping controller, then the available inverter capacity after real power generation (41.5 MVAr) is utilised to improve the power transfer limit. The improvement in power transfer capacity is lower during the day than at night. However, Table 3 shows that the power transfer is 850 MW at night and 851 MW during the day. This happens because of the increase in PCC voltage to 1.1 p.u.

3.2. CASE-II

The improvement of the power transfer capacity depends on the reference value of the PCC voltage. During night-time with only the PCC voltage controller, the output power of the generator is 833 MW when the V_{PCC} is regulated to 1.01 p.u., which is greater than the reactive power controller output. During the day, the power transfer enhancement is very sensitive to the PCC voltage reference when PV systems generate minimum and maximum power.

The transient stability and power flow results are shown in Table 5 for this condition. When the PCC voltage controller operates with a damping controller, the rotor oscillations settle more quickly, but the transmitted power is not increased beyond 899 MW due to voltage overshoot.

Figure 6 shows the power transfer capacity of the system when PCC voltage is considered for reference generation during the day. The results show that during the night the improvement of the power transfer is achieved by using PCC voltage and damping controllers, and during the day the objective is achieved by using damping controllers alone. This was because during the night, the full inverter capacity was used to fulfil the objective, and during the day only part of the inverter capacity was used to increase the power transfer capacity due to the increase in PCC voltage.

4. EXPERIMENTAL VALIDATION

The hardware implementation was done for a three-phase system. For each phase, different transformers were used to couple the inverter to the grid. Each phase had its own separate driver circuit designed using IC 4047. This circuit also included a solar panel and a lead-acid battery. For the three driver circuits, power supply was provided by four 12 V batteries for each circuit. The proposed prototype hardware is shown in Figure 7, it consists of a grid, which is connected to the load. 440 V supply voltage was used as the grid, with lamps as a load. The proposed MLMFI was connected at the point of common coupling. The

Condition		Gen. bus power [MWAr]	Inf. bus power [MW]	PCC parameters Psolar [MW]	Qsolar [MWAr]	Vpcc [pu]
Daytime	Voltage controller	719	−786	91.0	−43.5	1.00
	only	815	−804	19.0	−13.0	1.00
	Voltage controller with	755	−817	91.0	−41.0	1.00
	damping controller	823	−813	19.0	−9.0	1.00
Nighttime	Voltage controller	789	−761	−1.5	−95.0	0.97
	only	833	−803	−0.3	46.8	1.01
	Voltage controller with	855	−824	−0.3	4.0	1.00
	damping controller	899	−866	−1.2	86.0	1.01

Table 5. Power and voltage for PCC voltage controller and damping controller.

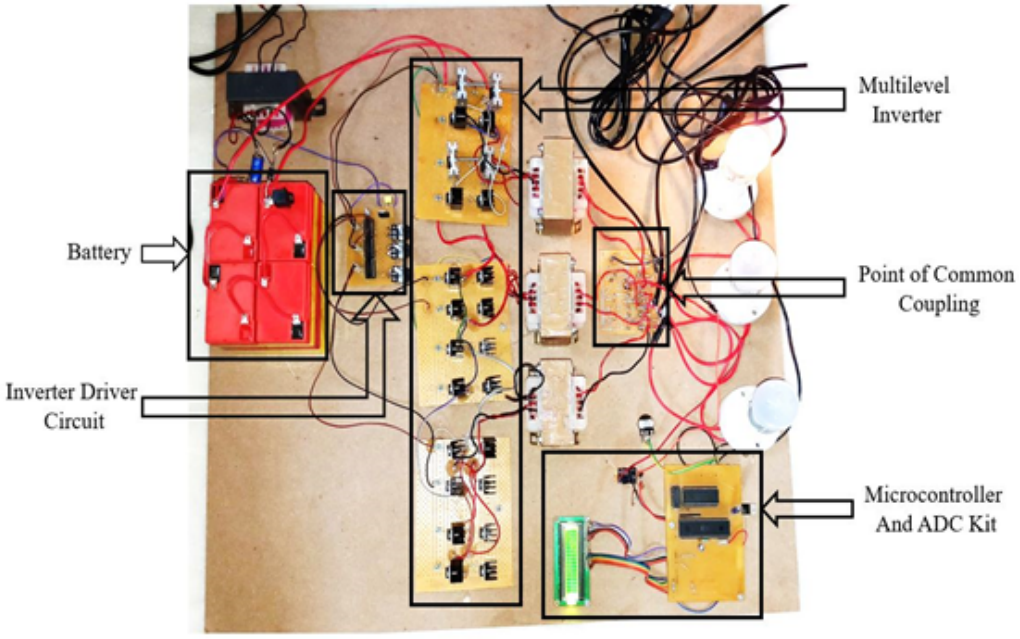

Figure 7. Experimental setup of MLMFI.

solar panels gave DC values as output. For converting DC to AC, a multilevel inverter was used. The multilevel inverter was configured using a MOSFET. The parameters of the experimental setup are listed in Table 6.

Parameter	Value
Grid L-L Voltage	440 V
DC Batteries	12 V 3 AH
Lamp Load	800 W
Microcontroller	$PIC16f877a$
MOSFET	IRFZ44

Table 6. Experimental setup parameters

Two H-bridges were used in the inverter for 5-level output voltage. The output of the inverter was 24 VAC, which was then stepped up to 230 V using a transformer. The transformer was shunt connected to the grid at the point of common coupling. The results were tested on a power analyser for a three phase output of three separate phases. The load connected to the system was approximately an 800 W lamp load. The three-phase, three wire system was selected on the power analyser. The data were collected with and without the MLMFI.

Figure 8 shows the voltage and current at the point of common coupling when the MLMFI was connected to the grid. Figure 8 shows that the voltage of the system increased to 431.3 V. The output waveform was almost sinusoidal because of the LCL filter effect, and the total harmonic distortion was 1.11 %.

From Figure 8, it can be seen that the current reached 1.48 A with the help of the MLMFI. The active and reactive power at the point of common coupling for an 800 W load are shown in Figure 9.

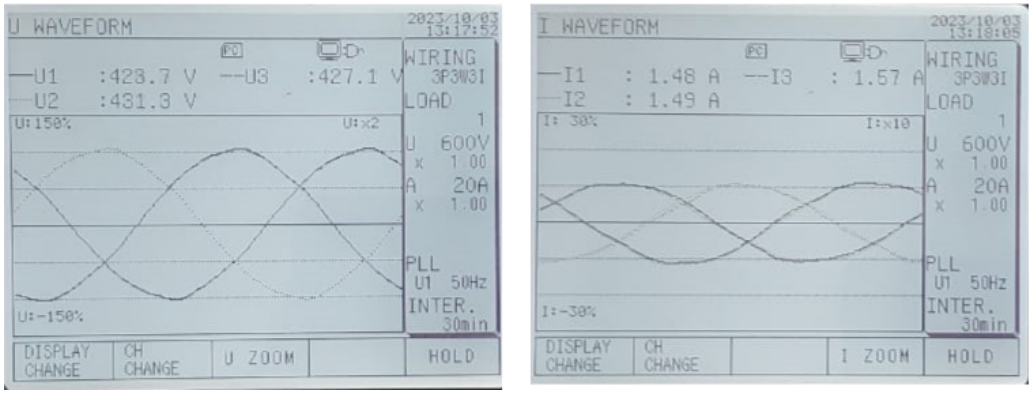

FIGURE 8. Voltage and current at PCC with PV-MLMFI system.

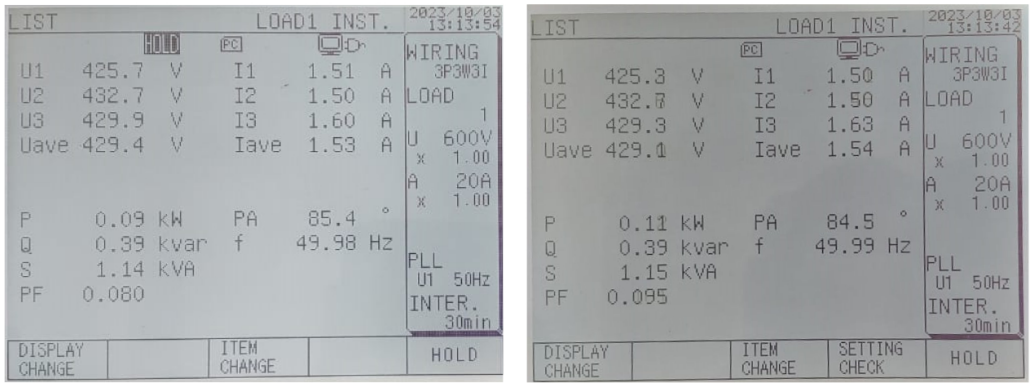

FIGURE 9. Grid power without and with PV-MLMFI system.

The active power without the MLMFI system at PCC was 0.09 kW, with a power factor of 0.80, which is low for any industrial application. It also shows the value of the output power of the proposed system using the MLMFI. It can be seen that with the use of MLMFI, there was an improvement in grid power capacity from 0.09 kW to 0.11 kW. The reactive power was supplied by the MLMFI system to maintain the voltage within limits. From these power values, it is clear that by using this proposed system, there is an improvement in the power transfer capacity of the grid.

5. Conclusions

This article presents the modelling of MLMFI and its controller to improve the active power transfer capability of a transmission network. It is verified that the multilevel inverter is best suited for solar array integration and power transfer capability improvement. When the solar array is idle at the night, the proposed controller uses the full capacity of the inverter to compensate for reactive power, and during the day it uses the remaining capacity of the inverter after real power generation. This new controller enabled the multilevel inverter to perform multiple operations, hence the name multifunction inverter. The MLMFI-based PV system improved the power transfer capability of the transmission line from 730 MW to 899 MW at night and from 719 MW to 823 MW during the day. This represents a 23 % increase in the power transfer capacity of the transmission grid. In addition, the voltage profile of the system improved by 9.5 %. There is a power factor improvement from 0.80 to 0.95 achieved with the proposed system. The proposed novel controller for multilevel inverters for PV grid integration will eliminate the need for additional investment in expensive FACTS devices.

References

[1] D. Zhu, S. Zhou, X. Zou, et al. Small-signal disturbance compensation control for LCL-type grid-connected converter in weak grid. *IEEE Transactions on Industry Applications* **56**(3):2852–2861, 2020. https://doi.org/10.1109/TIA.2020.2980729

[2] F. Blaabjerg, Y. Yang, D. Yang, X. Wang. Distributed power-generation systems and protection. *Proceedings of the IEEE* **105**(7):1311–1331, 2017. https://doi.org/10.1109/JPROC.2017.2696878

[3] Int. Energy Agency. *Energy from the desert: Very large scale PV power plants for shifting to renewable energy future*. Paris, France, 2015.

[4] Y. Song, X. Wang, F. Blaabjerg. Impedance-based high-frequency resonance analysis of DFIG system in weak grids. *IEEE Transactions on Power Electronics* **32**(5):3536–3548, 2017. https://doi.org/10.1109/TPEL.2016.2584118

[5] T. Wen, D. Zhu, X. Zou, et al. Power coupling mechanism analysis and improved decoupling control for virtual synchronous generator. *IEEE Transactions*

on Power Electronics **36**(3):3028–3041, 2021. https://doi.org/10.1109/TPEL.2020.3017254

[6] N. Flourentzou, V. G. Agelidis, G. D. Demetriades. VSC-based HVDC power transmission systems: An overview. *IEEE Transactions on Power Electronics* **24**(3):592–602, 2009. https://doi.org/10.1109/TPEL.2008.2008441

[7] P. Rao, M. L. Crow, Z. Yang. STATCOM control for power system voltage control applications. *IEEE Transactions on Power Delivery* **15**(4):1311–1317, 2000. https://doi.org/10.1109/61.891520

[8] K. Bisht, D. Kumar, K. Bedi. Enhancement of power transfer capacity and transmission efficiency using SSSC. *IJEAT* **9**(3):2846–2850, 2020. https://doi.org/10.35940/ijeat.C5999.029320

[9] S. Santhanalakshmi, S. Divya. Enhancement of power transfer ability in transmission and distribution line using TCSC. *IJEAT* **S**(2):4167–4171, 2020. https://doi.org/10.26637/MJM0S20/1086

[10] L. Xu, P. Dong, M. Liu. A comparative analysis of the interaction between different FACTS and HVDC. In *2012 IEEE Power and Energy Society General Meeting*, pp. 1–5. IEEE, San Diego, CA, USA, 2012. https://doi.org/10.1109/PESGM.2012.6344993

[11] Y. Jiang, J. Sun, W. Hu, et al. Analysis and suppression of interaction between STATCOM and voltage-source inverter in islanded micro-grid. In *2015 IEEE Energy Conversion Congress and Exposition (ECCE)*, pp. 6858–6863. IEEE, Montreal, QC, Canada, 2015. https://doi.org/10.1109/ECCE.2015.7310620

[12] H. J. Kim, T. Nam, K. Hur, et al. Dynamic interactions among multiple FACTS controllers – a survey. In *2011 IEEE Power and Energy Society General Meeting*, pp. 1–8. IEEE, Detroit, MI, USA, 2011. https://doi.org/10.1109/PES.2011.6039300

[13] M. Amin, M. Molinas. Understanding the origin of oscillatory phenomena observed between wind farms and HVdc systems. *IEEE Journal of Emerging and Selected Topics in Power Electronics* **5**(1):378–392, 2017. https://doi.org/10.1109/JESTPE.2016.2620378

[14] A. Moawwad, V. Khadkikar, J. L. Kirtley. Photovoltaic power plant as FACTS devices in multi-feeder systems. In *IECON 2011 – 37th Annual Conference of the IEEE Industrial Electronics Society*, pp. 918–923. IEEE, Melbourne, VIC, Australia, 2011. https://doi.org/10.1109/IECON.2011.6119433

[15] R. K. Varma, R. Salehi. SSR mitigation with a new control of PV solar farm as STATCOM (PV-STATCOM). *IEEE Transactions on Sustainable Energy* **8**(4):1473–1483, 2017. https://doi.org/10.1109/TSTE.2017.2691279

[16] R. K. Varma, S. A. Rahman, T. Vanderheide. New control of PV solar farm as STATCOM (PV-STATCOM) for increasing grid power transmission limits during night and day. *IEEE Transactions on Power Delivery* **30**(2):755–763, 2015. https://doi.org/10.1109/TPWRD.2014.2375216

[17] T.-T. Ku, C.-H. Lin, C.-T. Hsu, et al. Enhancement of power system operation by renewable ancillary service. *IEEE Transactions on Industry Applications* **56**(6):6150–6157, 2020. https://doi.org/10.1109/TIA.2020.3020782

[18] IEEE. IEEE recommended practice and requirements for harmonic control in electric power systems, IEEE Std. 519-2014 (Revision of IEEE Std 519-1992), pp.1-29, June 2014. https://standards.ieee.org/standard/519-2014.html.

[19] K. M. Nathgosavi, P. M. Joshi. Possibility study of PV-STATCOM with CHB multilevel inverter: A review. In *Information and Communication Technology for Intelligent Systems*, vol. 195. Springer, Singapore, 2021. https://doi.org/10.1007/978-981-15-7078-0_56

[20] S. Kundu, S. Banerjee. An improved SHM-PAM technique for three-phase five-level CHB inverter utilizing both quarter-wave and half-wave symmetry waveforms to fulfill some important voltage harmonic standards. *IEEE Transactions on Industry Applications* **57**(6):6246–6260, 2021. https://doi.org/10.1109/TIA.2021.3116217

[21] H. P. Vemuganti, D. Sreenivasarao, S. K. Ganjikunta, et al. A survey on reduced switch count multilevel inverters. *IEEE Open Journal of the Industrial Electronics Society* **2**:80–111, 2021. https://doi.org/10.1109/OJIES.2021.3050214

[22] H. Li, Y. Zeng, B. Zhang, et al. An improved H5 topology with low common-mode current for transformerless PV grid-connected inverter. *IEEE Transactions on Power Electronics* **34**(2):1254–1265, 2019. https://doi.org/10.1109/TPEL.2018.2833144

[23] G. Valverde, T. Van Cutsem. Model predictive control of voltages in active distribution networks. *IEEE Transactions on Smart Grid* **4**(4):2152–2161, 2013. https://doi.org/10.1109/TSG.2013.2246199

[24] A. Gabash, P. Li. Active-reactive optimal power flow for low-voltage networks with photovoltaic distributed generation. In *2012 IEEE International Energy Conference and Exhibition (ENERGYCON)*, pp. 381–386. Florence, Italy, 2012. https://doi.org/10.1109/EnergyCon.2012.6347787

[25] C. L. Bhattar, M. A. Chaudhari. Centralized energy management scheme for grid connected DC microgrid. *IEEE Systems Journal* **17**(3):3741–3751, 2023. https://doi.org/10.1109/JSYST.2022.3231898

[26] S. Bolognani, S. Zampieri. A distributed control strategy for reactive power compensation in smart microgrids. *IEEE Transactions on Automatic Control* **58**(11):2818–2833, 2019. https://doi.org/10.1109/TAC.2013.2270317

[27] R. K. Varma, E. M. Siavashi. PV-STATCOM: A new smart inverter for voltage control in distribution systems. *IEEE Transactions on Sustainable Energy* **9**(4):1681–1691, 2018. https://doi.org/10.1109/TSTE.2018.2808601

[28] E. Can, H. H. Sayan. Development of fractional sinus pulse width modulation with beta gap on three step signal processing. *International Journal of Electronics* **110**(3):527–546, 2023. https://doi.org/10.1080/00207217.2022.2040056

[29] E. Can. Extra control coefficient additive ECCA-PID for control optimization of electrical and mechanic system. *Acta Polytechnica* **62**(5):522–530, 2022. https://doi.org/10.14311/AP.2022.62.0522

[30] E. Can. The application of multi-phase power distribution line with pure energy conversion. *Jurnal Kejuruteraan* **31**(2):193–199, 2019. https://doi.org/10.17576/jkukm-2019-31(2)-02

[31] E. Can, H. H. Sayan. The increasing harmonic effects of SSPWM multilevel inverter controlling load currents investigated on modulation index. *Tehnički vjesnik* **24**(2):397–404, 2017. https://doi.org/10.17559/TV-20151020134629

[32] G. Mokhtari, A. Ghosh, G. Nourbakhsh, G. Ledwich. Smart robust resources control in LV network to deal with voltage rise issue. *IEEE Transactions on Sustainable Energy* **4**(4):1043–1050, 2013. https://doi.org/10.1109/TSTE.2013.2265100

[33] L. Collins, J. K. Ward. Real and reactive power control of distributed PV inverters for overvoltage prevention and increased renewable generation hosting capacity. *Renewable Energy* **81**:464–471, 2015. https://doi.org/10.1016/j.renene.2015.03.012

[34] K. Turitsyn, P. Sulc, S. Backhaus, M. Chertkov. Options for control of reactive power by distributed photovoltaic generators. *Proceedings of the IEEE* **99**(6):1063–1073, 2011. https://doi.org/10.1109/JPROC.2011.2116750

[35] E. Demirok, P. C. González, K. H. B. Frederiksen, et al. Local reactive power control methods for overvoltage prevention of distributed solar inverters in low-voltage grids. *IEEE Journal of Photovoltaics* **1**(2):174–182, 2011. https://doi.org/10.1109/JPHOTOV.2011.2174821